9th International Conference on Fracture Mechanics of Concrete and Concrete Structures
FraMCoS-9
V. Saouma, J. Bolander, and E. Landis (Eds)
DOI 10.21012/FC9.020

A WEAKEST LINK FAILURE MODEL OF POLYCRYSTALLINE MEMS STRUCTURES

JIA-LIANG LE* **AND ROBERTO BALLARINI‡**

*University of Minnesota
Minneapolis, MN, USA
e-mail: jle@umn.edu

‡University of Houston
Houston, TX, USA
e-mail: rballari@central.uh.edu

Key words: Weakest link model, Size effect, Weibull statistics, MEMS devices

Abstract. MEMS devices typically need to be designed against a very low failure probability, which is beyond the capacity of histogram testing. Therefore, the understanding of the probabilistic failure of MEMS devices is crucial for the design process. Currently available probabilistic models for predicting the strength statistics of MEMS structures are based on classical Weibull statistics. Significant advances in experimental techniques for measuring the strength of MEMS devices have produced data that have unambiguously demonstrated the inadequacy of the Weibull distribution. This paper presents a robust probabilistic model for the strength distribution of polycrystalline silicon (poly-Si) MEMS structures. The overall failure probability of the structure is related to the failure probability of each material element along its sidewalls through a weakest-link statistical model. The failure statistics of the material element is determined by both the intrinsic random material strength and the random stress field induced by the sidewall geometry. Different from the classical Weibull statistics, the present model accounts for structures consisting of a finite number of material elements, and it predicts an intricate scale effect on their failure statistics. It is shown that the model agrees well with the measured strength distributions of poly-Si MEMS specimens of different sizes. The present model also explicitly relates the strength distribution to the size effect on the mean structural strength, and therefore provides an efficient means of determining the failure statistics of MEMS structures.

1 INTRODUCTION

The early development of Microelectromechanical Systems (MEMS) technology focused on devices that were subjected to relatively small stress and stain, and therefore structural reliability was not a primary consideration for the device design. These devices include the silicon structural components contained in the guts of Analog Devices' air bag accelerometer that are protected also from potential environment-induced material degradation by hermetic sealing. The failure of but one of 1,300 of these devices when subjected to mechanical shock and a range of temperatures led to their assessment as structurally highly reliable [3]. But note that in applications that require extremely high reliability, a probability of fracture of 1/1300 may not suffice. The Texas Instruments (TI) Digital Micromirror Device (DMD) is another celebrated device consisting of hundreds of thousands aluminum mirrors that was tested in excess of one trillion cycles without a single failure [18]. In contrast

to voltage-compensated accelerometers such as those developed by Analog Devices do not operate near the strain limits, some devices are designed to operate at high mechanical power densities and/or large deformation levels, in which the applied stress and strain could reach the strength and strain limits [26]. Therefore, there has been a continuing interest in understanding the reliability of MEMS materials and structures [1, 20, 22, 26, 36].

The work-horse material used to fabricate surface micromachined MEMS devices is polycrystalline silicon (poly-Si) [2, 27]. The fracture strength of MEMS-scale poly-Si volumes is governed by processing-induced surface defects, and less commonly defects within the volume. The randomness of the surface flaws and the resulting spatial distribution of stress lead to a wide variation in the material's nominal tensile strength; from 1 GPa in direct tension to 6 GPa in the vicinity of stress-concentrating notches [1]. In direct tension the probability that all flaws including the largest are subjected to the highest stress is assured. In a notched specimen on the other hand the largest flaw may experience much lower values of stress, or alternatively the region of highest stress may contain relatively small flaws. It is nearly impossible to eliminate processing-induced defects in MEMS devices, which leads to the observed variability of fracture strength of MEMS devices [20, 22].

It has transpired that the proof testing is critical for reliability analysis of MEMS devices [13]. The main challenge in experimental investigation of structural reliability of MEMS devices is to due the fact that the design should target a failure probability on the order of 10^{-4} or lower [1]. Early histogram testing of MEMS materials involved small numbers of specimens due to the limitation of testing procedures (e.g. [14, 38–40]), which could not be used to determine the failure probability function. To facilitate more efficient histogram testing, a slack-chain tester was recently developed at the Sandia National Laboratories that allows sequential tension tests on a large number of specimens (~ 1000 specimens) in a short time [36]. However, the existing experimental approaches are still hampered by two difficulties: 1) it is cost prohibitive to experimentally determine the strength corresponding to a low failure probability (e.g. $P_f \approx 10^{-4}$) during the design process; and 2) it is unfeasible to perform histogram testing for MEMS devices of various kinds of geometries or subjected to different loading configurations since most experimental platforms are designed for specific types of specimen geometries and loading conditions. Therefore, fundamental understanding of the probabilistic failure of MEMS devices subjected to high levels of and/or different types of mechanical forces is needed.

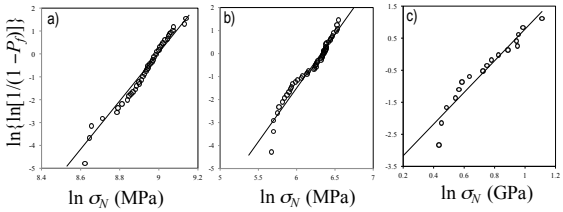

Figure 1: Measured strength distributions of MEMS structures made of: a) ta-C, b) single-crystal Si, and c) Poly-Si.

Currently available probabilistic models for the failure of MEMS structures are largely based on classical Weibull statistics. However, existing histogram testings have demonstrated that the strength distributions consistently deviate from those predicted by the two-parameter Weibull distribution. Fig. 1 presents, on the Weibull scale, the experimentally measured strength histograms of MEMS structures made of single-crystal Si [22], hydrogen-free tetrahedral amorphous carbon (ta-C) [20] and poly-Si [40]. Even with a limited number of specimens, it is seen that these histograms cannot be fitted by a straight line on the Weibull scale, which indicates the inadequency of the two-parameter Weibull distribution [16, 37]. An attempt to reconcile experimental histogram data with the Weibull approach was proposed using the three-parameter Weibull distribution [14, 36]. However, recent studies have pointed

out that for quasibrittle and brittle materials the three-parameter Weibull distribution would lead to incorrect scale effect on the mean structural strength [30, 33].

It has been generally agreed that the existing probabilistic models for brittle MEMS structures are still empirical in nature. This severely limits the predictability of these models. This paper presents a robust probabilistic model for MEMS structures that may lead to eliminating the need of less preferable costly proof testing approaches to guarantee the structural safety of devices that will operate at high mechanical power densities and/or large deformation levels.

2 GENERALIZED WEAKEST LINK MODEL FOR MEMS DEVICES

Consider a poly-Si MEMS specimen subjected to uniaxial tension, where the sidewalls of the specimen contain surface grooves resulted from the manufacturing process (Fig. 2a). These surface grooves can be approximated by V-notches [35, 36]. The applied tensile stress reaches its maximum value σ_N once a localized crack starts to propagate from one of these grooves. Therefore, the overall failure probability of the specimen can be calculated by using the weakest link model, i.e.:

$$P_f(\sigma_N) = 1 - \prod_{i=1}^{N} [1 - P_1(\sigma_N)] \qquad (1)$$

where the function $P_1(x)$ represents the probability of the propagation of a localized crack from one surface groove (V-notch). We consider that such a failure at the V-notch occurs when the the average tensile stress $\bar{\sigma}$ of the near-tip region attains the tensile strength f_t of the material. The average near-tip tensile stress is calculated as

$$\bar{\sigma} = r_c^{-1} \int_0^{r_c} \sigma_{yy}(x) \mathrm{d}x \qquad (2)$$

where $\sigma_{yy}(x)$ = elastic tensile stress along the notch ligament (Fig. 2b) and r_c = size of the near-tip region in which the average stress is computed. It is noted that this averaging procedure can be considered to take into account the interaction of the sub-scale damage inside the fracture process zone of the V-notch. Therefore, the material tensile strength f_t used here should be taken as the tensile strength of the material element of a size equal to the size of the fracture process zone (FPZ). In this study, we assume $r_c = 5$ nm, which is on the order of the estimated FPZ size of silicon [36, 41]. It should be noted that the value of r_c could be better determined by employing detailed atomistic calculations for the near-tip region, which provides insights into the various failure mechanisms of silicon crystals.

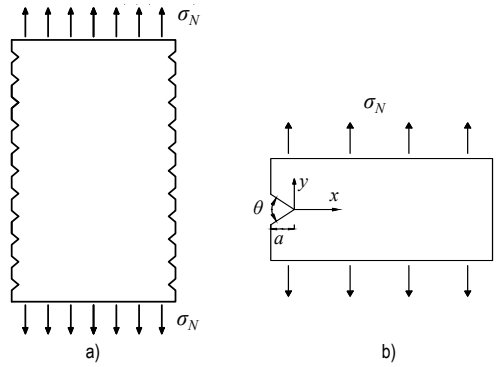

Figure 2: Analysis of poly-Si tension specimens: a) specimen geometry, and b) geometrical characterization of a surface groove.

The aforementioned failure criterion indicates that the overall tensile strength of the specimen can be calculated as

$$\sigma_N = f_t / s \qquad (3)$$

where s = dimensionless stress such that $\bar{\sigma} = \sigma_N s$. The probability of crack propagation from one surface groove can then be calculated as

$$P_1 = \text{Prob}(\bar{\sigma} \geq f_t) = \text{Prob}(f_t/s \leq \sigma_N) \qquad (4)$$

Eq. 4 indicates that the failure probability of one surface groove is governed by both material tensile strength as well as the stress field at the notch tip. Both of these quantities are subjected to a certain level of uncertainty. According to recent studies on the strength statistics of quasibrittle materials [8–10, 30], the probability distribution of the material tensile strength can

be approximated by a Gaussian-Weibull grafted distribution function:

$$F_{f_t}(x) = 1 - e^{-\langle x/s_1 \rangle^m} \quad (x \leq x_{gr}) \tag{5a}$$

$$F_{f_t}(x) = P_{gr} + \frac{r_f}{\delta_G \sqrt{2\pi}} \times \int_{x_{gr}}^{x} e^{-\frac{(x'-\mu_G)^2}{2\delta_G^2}} \mathrm{d}x' \quad (x > x_{gr}) \tag{5b}$$

where m = Weibull modulus (shape parameter), s_0 = Weibull scale parameter, μ_G, δ_G = mean and standard deviation of the Gaussian core, respectively, $P_{gr} = 1 - \exp[-(x_{gr}/s_0)^m]$ = grafting probability at which the Weibull tail ends, and r_f = normalizing parameter, which ensures that $F_{f_t}(\infty) = 1$. Furthermore, the probability density function (pdf) at the Weibull-Gaussian grafting point must be continuous, i.e. $\mathrm{d}P_{f_t}(x)/\mathrm{d}x|_{x=\sigma_{gr}^-} = \mathrm{d}P_{f_t}(x)/\mathrm{d}x|_{x=\sigma_{gr}^+}$.

The randomness of the dimensionless stress s is caused by the random geometry of the surface V-notch. By assuming that the V-notches along the sidewall are non-interacting, we may calculate the elastic field for a strip of the specimen that contains a V-notch on one of its sidewalls, as shown in Fig. 2b. It is noted that the V-notch on the other side does not affect the near-tip stress field of the V-notch on this side since the width of a typical MEMS specimen (on the order of microns) is much larger than the size of the near-tip region. Therefore, we only need to consider one V-notch to compute the near-tip elastic stress field. The geometry of the V-notch can be described by the notch angle θ and notch depth a. With knowing the probability distributions of these two geometrical parameters, we can perform a stochastic analysis of the near-tip stress field to obtain the probability distribution of the dimensionless stress, $F_s(x)$. It is noted that in this study we did not consider the random crystal orientation since it has recently been shown that the mismatch of silicon's (relatively low anisotropy) crystal orientation has a mild effect on the near-tip stress field [36].

By considering both material tensile strength and dimensionless stress field as random variables, Eq. 4 can be re-written as:

$$P_1(\sigma_N) = \int_0^\infty F_{f_t}(x\sigma_N) f_s(x) \mathrm{d}x \tag{6}$$

where $f_s(x) = \mathrm{d}F_s(x)/\mathrm{d}x$ = probability density function (pdf) of dimensionless stress s. The probability distribution of the tensile strength of the entire specimen can be computed as:

$$P_f(\sigma_N) = 1 - \left[1 - \int_0^\infty F_{f_t}(x\sigma_N) f_s(x) \mathrm{d}x\right]^{2n} \tag{7}$$

where n = number of V-notches along one sidewall. It should be noted that here we have assumed that the strength of each material element is statistically independent. Such an assumption is reasonable because the size of the V-notch is considerably larger than the FPZ size, which is approximately on the same order of the autocorrelation length of random strength field for brittle and quasibrittle materials [10, 23].

3 COMPARISON WITH EXPERIMENTAL DATA

The recently developed high-throughput testing techniques have produced more complete information on the strength statistics of MEMS devices including its scale effect. Fig. 3 shows the measured strength distributions of poly-Si tensile specimens of two gauge lengths (L_g = 20 and 70 μm) [36]. Both specimens have a nominal width of 2 μm. The specimens of 70 μm gauge length were tested using an on-chip tester [24], and the specimens of 20 μm gauge length were tested using a slack-chain tester [12]. The detailed experimental procedure for these histogram tests can be found in [24, 36]. Before comparing the test data with any probabilistic models, we note that the present data with a size ratio of 1: 3.5 may not be sufficient to fully justify the predictability of any model. Nevertheless, as will be shown later in this section, histograms of such a limited size

range have already indicated the limitations of the classical Weibull models, and the present model is shown to be capable of capturing some essential features of these experimental data.=

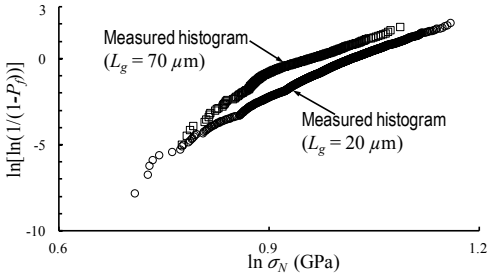

Figure 3: Measured strength distributions of poly-Si MEMS specimens of two gauge lengths.

Finite weakest link model

We now test the present probabilistic model against this set of experimental data. According to [36], there are approximately 50 surface grooves along one sidewall of the tensile specimen with a gauge length of 20 μm. Therefore, we may consider that on average each surface groove is contained in a strip of specimen with a length of 400 nm ($\sigma_N = 1$). To characterize the random notch geometry, we assume that the notch angle θ follows a uniform distribution bounded between 20° and 140° whereas the notch depth a follows the Type III extreme value distribution for the maximum value with an upper bound of 62 nm [36]. The cumulative distribution functions (cdfs) of θ and a can be written as

$$F_\theta(x) = \frac{x-20}{120} \quad (8)$$

$$F_a(x) = \exp\left[-\left(\frac{\langle 62-x\rangle}{28}\right)^{6.5}\right] \quad (9)$$

where $\langle x\rangle = \max(x,0)$. Though the assumed probability distribution function of the notch depth extends to unrealistic negative values, the left tail for the negative notch depth is extremely short (i.e. $F_a(0) = 6.7\times10^{-77}$). It is also noted that the aforementioned bounds of notch angle and depth ensure that, for any combination of notch angle and depth sampled from the above distributions, the V-notch can always be contained in a 400 nm long strip of the specimen. Based on Eqs. 8 and 9, we perform stochastic elastic analysis of the stress field for the strip of the tensile specimen with the random notch angle and depth. In the simulation, the poly-Si material is modeled as an isotropic material with a Young Modulus $E = 156$ GPa and a Poisson ratio $\nu = 0.22$ [36].

The cdf of material tensile strength, $F_{f_t}(x)$, needs to calibrated by optimum fits of the measured strength histograms. Since we have strength histograms of specimens of two gauge lengths, we can choose one of them to calibrate the function $F_{f_t}(x)$ and compare the other one with the model prediction. Table 1 presents the statistical parameters of $F_{f_t}(x)$ calibrated by optimum fits of 1) strength histogram of specimens of 20 μm gauge length, and 2) strength histogram of specimens of 70 μm gauge length. It can be seen that these two calibrations yield very similar values of the parameters of $F_{f_t}(x)$, which indicates the robustness of the present model.

Table 1: Calibrated statistical parameters of the finite weakest link model

Specimens	m	s_0	μ_G	δ_G
$L_g = 20$ μm	64	12.60	19.96	3.50
$L_g = 70$ μm	65	12.79	19.84	3.40

s_0, μ_G, δ_G are in GPa.

Fig. 4 compares the measured strength histogram of the other set of specimens with the prediction by the present model. It is seen that, regardless of choice of calibration specimens, the present model can predict reasonably well the strength distribution of specimens of the other gauge length. This indicates that the present model is able to capture the size effect on the strength distribution of poly-Si MEMS specimens, which is essential for reliability-based design extrapolation across different specimen sizes. It is interesting to note

that the calibrated mean strength of each material element is about 20 GPa, which is of the order of the theoretical strength of silicon [19].

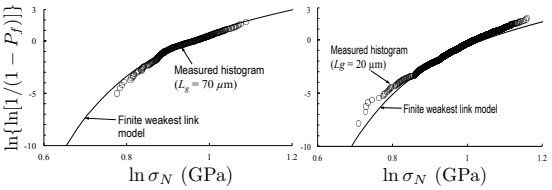

Figure 4: Comparison between the experimental measured strength distribution with the prediction by the finite weakest link model.

It should also be pointed out that the calibration of function $F_{f_t}(x)$ depends on the choice of the size of the near-tip region r_c. As mentioned earlier, we choose $r_c = 5$ nm based on the knowledge of the FPZ size, and it gives a reasonable estimation of the mean strength of the material element of poly-Si. The choice of r_c would change the value of the dimensionless stress s, but not the functional form of the overall failure probability $P_f(\sigma_N)$. Therefore we expected that Eq. 7 can still match the histograms well with a different set of parameters of $F_{f_t}(x)$.

Two-parameter Weibull distribution

As a comparison, we also test the commonly used two-parameter Weibull distribution against this data set. The two-parameter Weibull distribution for tensile specimens can be written as [42, 43]

$$P_{w2}(\sigma_N) = 1 - \exp\left[-2n(\sigma_N/s_w)^{m_w}\right] \quad (10)$$

where s_w = Weibull scaling parameter and m_w = Weibull modulus. The values of s_w and m_w can be easily obtained by fitting the measured strength histogram on the Weibull scale by a straight line. Similar to the aforementioned calibration procedure, we determine s_w and m_w by optimum fitting either one of the two strength histograms and compare the other histogram with that predicted by Eq. 10.

Table 2: Calibrated statistical parameters of the two-parameter and three-parameter Weibull distributions

Specimens	m_w	s_w	m_1	s_1	σ_0
$L_g = 20$ μm	18.25	3.59	5.78	2.22	1.78
$L_g = 70$ μm	18.45	3.61	3.03	3.66	2.08

s_w, s_1, σ_0 are in GPa.

Table 2 lists the values of s_w and m_w determined by fitting the strength histograms of specimens of either of the two gauge lengths. It can be seen that the calibrated values mildly depend on which strength histogram is used for fitting. Fig. 5 presents the predicted strength histogram of specimens of the other gauge length by the two-parameter Weibull distribution with the experimental data. Clearly, for either of the two calibrations, the two-parameter Weibull distribution cannot well predict the strength distribution of specimens. The physical reason for such a deviation is that for these two sets of test specimens the number of failure points (i.e. V-notches) inside the specimen is not very large. Therefore, the two-parameter Weibull distribution, which is derived on the basis of extreme value statistics (or infinite weakest link model), is insufficient.

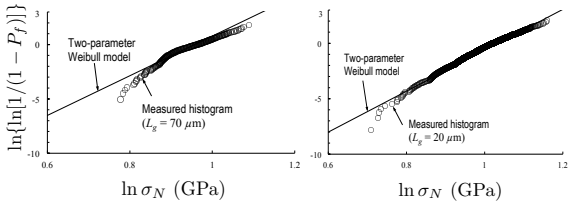

Figure 5: Comparison between the experimental measured strength distribution with the prediction by the two-parameter Weibull distribution.

Three-parameter Weibull distribution

The three-parameter Weibull distribution has recently been proposed as a remedy for the two-parameter Weibull distribution, in which it introduces a finite strength threshold under which the structure has a zero failure probability. The three-parameter Weibull distribution for tensile

specimens can be written as

$$P_{w3}(\sigma_N) = 1 - \exp\left[-2n\frac{\langle\sigma_N - \sigma_0\rangle^{m_1}}{{s_1}^{m_1}}\right] \quad (11)$$

where σ_0 = strength threshold. We can determine m_1, s_1 and σ_0 by fitting the strength histogram of specimens of any size. Table 2 presents the two sets of values of these three parameters by optimum fitting of the strength histograms of specimens of 20 μm and 70 μm gauge lengths, respectively. It can be seen that, compared to the present model and the two-parameter Weibull model, the calibration result of the three-parameter Weibull model is more strongly dependent on the choice of the calibration specimen.

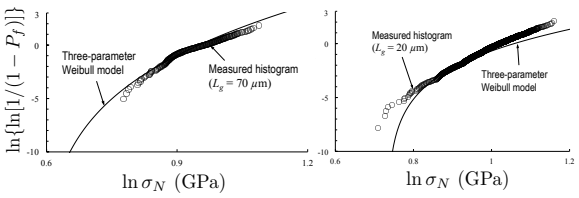

Figure 6: Comparison between the experimental measured strength distribution with the prediction by the three-parameter Weibull distribution.

Fig. 6 compares the predicted strength histogram of specimens that is not used for fitting with the experimental result. It is interesting to see that, if we calibrate m_1, s_1 and σ_0 based on the strength histogram of specimens of 20 μm gauge length, Eq. 11 can predict well the strength distribution of specimens of 70 μm gauge length. On the contrary, if we calibrate m_1, s_1 and σ_0 based on the strength histogram of specimens of 70 μm gauge length, Eq. 11 fails to predict the strength distribution of specimens of 20 μm gauge length. This illustrates the lack of robustness of the three-parameter Weibull distribution for prediction of the size dependence of the failure statistics of specimens.

Based on the foregoing analysis, we may conclude that the aforementioned comparison with the experiment data on poly-Si tensile specimens of two different gauge lengths favors the present finite weakest link model over the classical two- and three-parameter Weibull distributions, even though the size range of the experimental data is narrow. It is interesting to further compare the strength distributions of specimens for a wider range of gauge lengths predicted by the present finite weakest link model and the three-parameter Weibull distribution, as shown in Fig. 7. It can be seen that for $n = 50$ two models give a reasonably similar prediction of the failure probability except for the left tail since these two models are calibrated based on the test results for specimens of 20 μm gauge length. At the small size limit, it is observed that two models only differ at the high-probability regime and the extreme far left tail. At the large-size limit, these two models give a similar prediction for the high-probability regime and they deviate from each other significantly at the low probability regime.

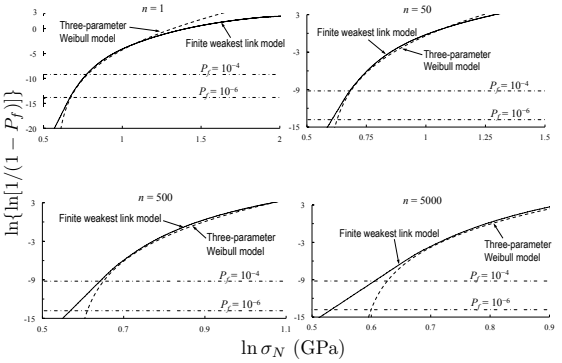

Figure 7: Comparison of strength distributions of poly-Si MEMS specimens of different gauge lengths by the finite weakest model and the three-parameter Weibull distribution.

The aforementioned observation can be explained by the fact that the strength distribution for the high probability regime of large-size structures is determined by the strength distribution for the low probability regime of small-size structures, which is an essential feature of the weakest link model. As seen in Fig. 7b, the finite weakest link model and the three-parameter Weibull distribution yield a similar prediction for the bulk part of the strength distribution for $n = 50$. Therefore, we expect that

these models would also lead to a similar prediction for the strength statistics at the moderately low probability regime for $n = 1$, as seen Fig. 7a. Meanwhile, it is observed that these two models differ from each other at the extremely low failure probability regime as well as the high probability regime. As n increases, we see that the difference in prediction by these models start to propagate into the intermediate probability regime. This is because that the difference in the tail behaviors predicted by these two models is manifested in the different behavior of the bulk part of the strength distribution as the specimen size increases.

4 MEAN SIZE EFFECT ANALYSIS

One of the salient features of the finite weakest link model (Eq. 7) is that it predicts a strong size dependence of strength distribution of MEMS devices, which is expected to lead to a size effect on the mean structural strength. In this section, we explore the relationship between this mean size effect and the strength distribution. This relationship would allow us to bypass the laborious histogram testing to determine the strength distribution of MEMS devices. Instead, we would just need to test the mean strength of MEMS devices of four to five sizes. In this study, we formulate this relationship for uniaxial tension specimens, while the same formulation can directly be applied to structures of other geometries or under other loading configurations.

Based on Eq. 7, the mean structural strength can be calculated as

$$\bar{\sigma}_N = \int_0^\infty \left[1 - \int_0^\infty F_{f_t}(x\sigma_N) f_s(x) \mathrm{d}x\right]^{2n} \mathrm{d}\sigma_N \tag{12}$$

The randomness of V-notch geometry can be accurately determined from the examination of the sidewall surface grooves [36], from which the probability distribution of the dimensionless stress, $f_s(x)$, can be calculated. Therefore, the essential problem is to determine the cdf of the material element strength, i.e. $F_{f_t}(x)$.

Fig. 8 presents the size effect on the tensile specimens calculated by Eq. 12, where $F_{f_t}(x)$ is calibrated based on the strength histogram of specimen of 20 μm gauge length. It is seen that, on the log-log scale, the mean size effect curve deviates from the Weibull size effect due to the fact that there are a finite number of V-notches along the sidewalls. As expected, when the specimen length becomes large, the mean size effect does follow the Weibull size effect represented by a straight line on the log-log scale. Though Eq. 12 cannot be integrated analytically, we may construct a general approximate equation for $\bar{\sigma}_N$ by anchoring at the small- and large-size limits [6, 7, 30]:

$$\bar{\sigma}_N = \mu_0 \left[\frac{n_1}{n} + \left(\frac{n_2}{n}\right)^{r/q}\right]^{1/r} \tag{13}$$

where μ_0 = mean strength of material element, and n_1, n_2, r, and q are constants. Let us denote $C_1 = \mu_0^r n_1$ and $C_2 = \mu_0^q n_2$. Now we relate these constants to the probability distribution function of material strength $F_{f_t}(x)$. Based on Eqs. 5a and 5b, $F_{f_t}(x)$ can uniquely be defined by the following four parameters: the Weibull modulus m, the Weibull scaling parameter s_0, the mean of the Gaussian core μ_G, and the standard deviation of the Gaussian core δ_G.

At the large size limit, the strength distribution of the structure must converge to the Weibull distribution (Eq. 14) [28], i.e.:

$$P_f(\sigma_N) = 1 - \exp\left[-2nM_m(\sigma_N/s_0)^m\right] \tag{14}$$

where $M_m = \int_0^\infty x^m f_s(x)\mathrm{d}x = m$th moment of probability distribution function $F_s(x)$. The corresponding mean structural strength can be easily obtained:

$$\bar{\sigma}_N = (2n)^{-1/m} s_0 \Gamma(1 + 1/m) M_m^{-1/m} \tag{15}$$

On the other hand, as $n \to \infty$, Eq. 13 reduces to $\bar{\sigma}_N \approx \mu_0 (n_2/n)^{1/q}$. Comparing this expression with Eq. 15, we obtain

$$m = q \tag{16}$$

$$s_0 = (2M_m)^{-1/m} C_2^{1/q} \Gamma^{-1}(1 + 1/m) \tag{17}$$

This implies that constants q and C_2 are directly related to the Weibull modulus and the Weibull scaling parameter.

At the small-size limit, we consider that the entire specimen consists of only two V-notches, one on each sidewall. It is well expected that the Weibull tail can be neglected for calculating the mean strength. Therefore, we may replace the the grafted strength distribution of F_{f_t} by a Gaussian distribution to compute the mean strength at the small-size limit, i.e.:

$$\bar{\sigma}_N|_{n=2} = \int_0^\infty \left[1 - \int_0^\infty \Phi(x')f_s(x)\mathrm{d}x\right]^2 \mathrm{d}\sigma_N \tag{18}$$

where $x' = (x\sigma_N - \mu_G)/\delta_G$ and $\Phi(x) =$ standard Gaussian distribution. Meanwhile, we can also calculate the gradient of $\bar{\sigma}_N$ with respect to the number of V-notches at the small-size limit:

$$\frac{\mathrm{d}\bar{\sigma}_N}{\mathrm{d}n}|_{n=2} = \int_0^\infty \left[1 - \int_0^\infty \Phi(x')f_s(x)\mathrm{d}x\right]^2 \times \ln\left[1 - \int_0^\infty \Phi(x')f_s(x)\mathrm{d}x\right] \mathrm{d}\sigma_N \tag{19}$$

These two small-size asymptotes of Eq. 13 can be written as

$$\bar{\sigma}_N|_{n=2} = \left[\frac{C_1}{2} + \left(\frac{C_2}{2}\right)^{r/q}\right]^{1/r} \tag{20}$$

$$\frac{\mathrm{d}\bar{\sigma}_N}{\mathrm{d}n}|_{n=2} = -\frac{1}{r}\left[\frac{C_1}{2} + \left(\frac{C_2}{2}\right)^{r/q}\right]^{1/r-1} \times \left[\frac{C_1}{4} + \frac{r}{2q}\left(\frac{C_2}{2}\right)^{r/q}\right] \tag{21}$$

It is clear that, by equating Eq. 18 to Eq. 20 and Eq. 19 to Eq. 21, we can calculate μ_G and δ_G from C_1, C_2, r and q. Therefore, if we obtain a size effect curve on the mean structural strength of MEMS devices fitted by Eq. 13, we can use the foregoing formulation to determine s_0, m, μ_G and δ_G, from which we can further calculate the corresponding strength distributions.

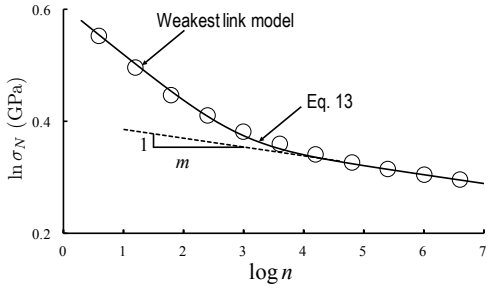

Figure 8: Comparison of the mean size effect curves calculated by the finite weakest link model and Eq. 13.

The aforementioned formulation is now verified by using the current analysis of the poly-Si tension specimens. We use the calibrated the cdf of material tensile strength, i.e. s_0, m, μ_G and δ_G to calculate the approximate size effect curve on the mean strength through Eqs. 16 - 21. This approximate size effect curve is compared with the exact size effect curve calculated by using the finite weakest link model. Fig. 8 shows that they agree well with each other, which verifies the proposed relationship between the mean size effect curve and the strength distribution.

5 CONCLUSIONS

1. A finite weakest model is developed for strength distribution of poly-Si MEMS devices, which considers both the random material strength and random geometrical features of the specimen. The model is shown to be able to capture the measured strength histograms of poly-Si MEMS specimens of two gauge lengths. The present analysis indicates that the model can be calibrated by optimum fitting of either one of these two strength histograms, and the results are midly affected by the choice of the calibration specimens.

2. It is shown that the two-parameter Weibull distributions is inadequate for modeling the measured size effect on the strength histograms of poly-Si specimens. This is because the number of potential failure locations in the specimen is not large, thus violating the basic assumption of the Weibull distribution. The three-parameter Weibull distribution can improve the optimum

fitting. However, the model calibration is shown to be dependent on the choice of the calibration specimens, which severely limits its prediction capability.

3. The size dependence of strength statistics of MEMS structures indicates that the direct experimental validation of the strength distribution using histogram testing must involve specimens of a sufficiently large size range. Such a size effect test procedure eliminates the need for direct measurement of tail distribution, since the far-left tail behavior is manifested by the bulk part of the strength distribution of large-size specimens.

4. The finite weakest link model predicts an intricate size effect on the strength distribution as well as the mean structural strength. It is shown that the mean size effect and the strength distribution are related to each other. This relationship provides us a new way to determine the strength statistics of MEMS structures, which is far more efficient than the conventional histogram testing.

REFERENCES

[1] Ballarini, R. (1998) *Contributive Research & Development Volume 130: The Role of Mechanics in Microelectromechanical Systems (MEMS) Technology*, Air Force Research Laboratory Report, Rep. No. AFRL-ML-WP-TR-1998-4209.

[2] Ballarini, R., Kahn, H., Heuer, A. H., de Boer, M. P. and Dugger, M. T. (2003) "MEMS structures for on-chip testing of mechanical and surface properties of thin films." in Comprehensive Structural Integrity, Edited by W. Gerberich and W. Yang, Vol. 8, Elsevier, 325–356.

[3] Bart, S., Chang, J., Core, T. and Foster, L. (1995) "Design rules for a reliable surface micromachined IC sensor." *IEEE Int. Reliability Phys. Proc.*, 311–317.

[4] Bazant, M. Z. (2000) "The largest cluster in subcritical percolation." *Phys. Rev. E*, 62, 1660–1669.

[5] Bazant, M. Z. (2002) "Stochastic renormalization group in percolation." *Physica A*, 316, 451–477.

[6] Bažant, Z. P. (2004) "Scaling theory of quaisbrittle structural failure." *Proc. Nat'l. Acad. Sci., USA* 101 (37), 13397-13399.

[7] Bažant, Z. P. (2005) *Scaling of Structural Strength*, 2nd Ed., Elsevier, London.

[8] Bažant, Z. P., Le, J.-L., and Bazant, M. Z. (2009) "Scaling of strength and lifetime distributions of quasibrittle structures based on atomistic fracture mechanics" *Proc. Nat'l. Acad. Sci., USA*, 106, No. 28, 11484-11489.

[9] Bažant, Z.P., and Pang, S.-D. (2006). "Mechanics based statistics of failure risk of quasibrittle structures and size effect on safety factors." *Proc. Nat'l. Acad. Sci., USA* 103 (25), pp. 9434–9439.

[10] Bažant, Z. P., and Pang, S. D. (2007) "Activation energy based extreme value statistics and size effect in brittle and quasibrittle fracture." *J. Mech. Phys. Solids*, 55, pp. 91–134.

[11] Bažant, Z. P. and Planas, J. (1998) *Fracture and Size Effect in Concrete and Other Quasibrittle Materials*, CRC Press.

[12] Boyce, B. L. (2010) "A sequential tensile method for rapid characterization of extreme-value behavior in micro fabricated materials." *Exp. Mech.*, 50, 993–997.

[13] Boyce, B. L., Ballarini, R. and Chasiotis, I. (2008) "An argument for proof testing brittle microsystems in high-reliability applications." *J. Micromech. Microeng.* 18, 117001 (4 pp).

[14] Boyce, B. L., Grazier, J. M., Buchheit, T. E., and Shaw, M. J., (2007) "Strength distributions in polycrystalline silicon MEMS" *J. Microelectromech. Syst.* 16(2), 179–190.

[15] Cannone Falchetto, A., Le, J.-L., Turos, M. I. and Marasteanu, M. O. (2014) "Indirect determination of size effect on strength of asphalt mixture at low temperatures", *Mater. Struc.*, Vol. 47, 1-2, 157–169.

[16] McCarty, A. and Chasiotis, I. (2007) "Description of brittle failure of non-uniform MEMS geometries." *Thin Solid Films*, vol. 515, no. 6, pp. 3267–3276.

[17] Christensen, R. M. (2013) *The Theory of Material Failure*, Oxford University Press.

[18] Douglass, M. R. (1998) "Lifetime estimates and unique failure mechanisms of the digital micromirror device (DMD)." *IEEE Int. Reliability Proc.*, 9–16.

[19] Dubois, S. M.-M., Rignanese, G. -M., Pardoen, T., and Charlier, J.-C. (2006). "Ideal strength of silicon: An *ab initio* study", *Phy. Rev. B.*, 74, 235203.

[20] Espinosa, H. D., Peng, B., Moldovan, N., Friedmann, T. A., Xiao, X., Mancini, D. C., Auciello, O., Carlisle, J. and Zorman, C. A. (2005). "A comparison of mechanical properties of three MEMS materials - Silicon carbide, ultrananocrystalline diamond, and hydrogen-free tetrahedral amorphous carbon (Ta-C)." *Proc. 11th Inter. Conf. on Frac.*, Turin, Italy.

[21] Fisher, R. A. and Tippett, L. H. C. (1928). "Limiting forms of the frequency distribution of the largest and smallest member of a sample." *Proc. Cambridge Philos. Soc.*, 24, 180–190.

[22] Fitzgerald, A. M., Pierce, D. M., Huigens, B. M. and White, C. D. (2009) "A general methodology to predict the reliability of single-crystal silicon MEMS devices." *J. Microelectromech. Systems*, 18(4), 962-970.

[23] Grassl, P. and Bažant, Z. P. (2009). "Random lattice-particle simulation of statistical size effect in quasi-brittle structures failing at crack initiation." *J. Eng. Mech. ASCE*, 135 (2), 85–92.

[24] Hazra, S. S., Baker, M. S., Beuth, J. L., and de Boer, M. P. (2009) "Demonstration of an in-situ on-chip tester." *J. Micromech. Microeng.*, vol. 19, no. 8, 082001.

[25] van der Hofstad, R. and Redig, F. (2006) "Maximal clusters in non-critical percolation and related models." *J. Statist. Phys.*, 122 (4), 671–703.

[26] Jiang, L. and Spearing, M. (2007) "A reassessment of materials issues in microelectromechanical systems (MEMS)." *J. Indian Inst. Sci.* 87(3), 363–385.

[27] Kahn, H., Ballarini, R., and Heuer, A. H. (2006) "Mechanical fatigue of polysilicon: Effects of mean stress and stress amplitude." *Acta Mater.* 54, 667–678.

[28] Le, J.-L., Ballarini, R., and Zhu, Z. (2015) "Modeling of probabilistic failure of polycrystalline silicon MEMS structures", *Journal of the American Ceramic Society*, 98(6), Feature Article, 1685–1697.

[29] Le, J.-L. and Bažant, Z. P. (2012) "Scaling of static fracture of quasibrittle structures: Strength, lifetime and fracture kinetics", *J. Appl. Mech.*, 79, 031006 (10 pp).

[30] Le, J.-L., Bažant, Z. P. and Bazant, M. Z. (2011) "Unified nano-mechanics based probabilistic theory of quasibrittle and brittle structures: I. strength, crack

growth, lifetime and scaling," *J. Mech. Phys. Solids*, 59, 1291–1321.

[31] Le, J.-L., Cannone Falchetto, A. and Marasteanu, M. O. (2013) "Determination of strength distribution of quasibrittle structures from size effect analysis", *Mechanics of Materials*, 66, 79–87.

[32] Munz, D., and Fett, T. (1999) *Ceramics: Mechanical Properties, Failure Behavior, Materials Selection*. Springer-Verlag, Berlin.

[33] Pang, S. D., Bažant, Z. P. and Le, J.-L. (2008) "Statistics of strength of ceramics: Finite weakest link model and necessity of zero threshold", *Int. J. Frac.*, 154, 131–145.

[34] Petersen, K. E. (1982) "Silicon as a mechanical material" *Proc. IEEE* 70, 420–457.

[35] Reedy, E. D. (2011) "Singular stress fields at the intersection of a grain boundary and a stress-free edge in a columnar polycrystal." *J. Appl. Mech.*, 78, 014502.

[36] Reedy, E. D., Jr., Boyce, B. L., Foulk, J. W., III, Field, R. V., Jr. de Boer, M. P., and Hazra, S. S. (2011) "Predicting fracture in micrometer-scale polycrystalline silicon MEMS structures." *J. Microelectromech. Syst.* 20(4), 922–932.

[37] Sharpe, W. N., Jadaan, O., and Beheim, G. M., Quinn, G. D. and Nemeth, N. N. (2005) "Fracture strength of silicon carbide microspecimens," *J. Microelectromech. Syst.*, vol. 14, no. 5, pp. 903–913.

[38] Tsuchiya T (2005) "Tensile testing of silicon thin films."*Fatigue and Fracture of Engineering Material and Structures* 28, 665–674.

[39] Tsuchiya, T., Tabata, O., Sakata, J., and Taga, Y. (1996) "Tensile testing of polycrystalline silicon thin films using electrostatic force grip," *Trans. Int. Elect. Engineers Japan*, vol. 116-E, No 10, pp 441-446.

[40] Tsuchiya, T., Tabata, O., Sakata, J., and Taga, Y. (1998) "Specimen size effect on tensile strength of surface-micromachined polycrystalline silicon thin films," *J. Microelectromech. Syst.*, vol. 7, p. 106-113.

[41] Yasutake, K., Iwata, M., Yoshii, K., Umeno, M. and Kawabe, H. (1986) "Crack healing and fracture strength of silicon crystals," *J. Mater. Sci.*, 21(6), 2185–2192.

[42] Weibull, W. (1939) "The phenomenon of rupture in solids." *In: Proceedings of Royal Swedish Institute of Engineering Research*, vol. 153, Stockholm. pp. 1–55.

[43] Weibull, W. (1951) "A statistical distribution function of wide applicability." *J. Appl. Mech. ASME*, 153 (18), 293–297.